AIAA JOURNAL
Vol. 35, No. 4, April 1997

Adaptive Remeshing for the k–ϵ Model of Turbulence

D. Pelletier* and F. Ilinca†
École Polytechnique de Montréal, Montréal, Québec H3C 3A7, Canada

An adaptive finite element method for solving incompressible turbulent flows using the k–ϵ model of turbulence is presented. Solutions are obtained in primitive variables using a highly accurate quadratic finite element on unstructured grids. Turbulence is modeled using the k–ϵ model of turbulence. Two error estimators are presented that take into account in a rigorous way the relative importance of the errors in velocity, pressure, turbulence variables, and eddy viscosity. The efficiency and convergence rate of the methodology are evaluated by solving problems with known analytical solutions. The method is then applied to turbulent free shear flows and predictions are compared to measurements.

Nomenclature

C_μ, C_1, C_2	= k–ϵ model constants
e	= error
f	= body force
h	= element size
K	= element in the mesh
k	= turbulent kinetic energy
n	= outward unit vector
$P(u)$	= production of turbulence
p	= pressure
u	= velocity vector
v, w, s	= test function
$\dot{\gamma}$	= strain rate tensor
δ	= element size for new mesh
ϵ	= turbulence dissipation
μ	= viscosity
ξ	= reduction coefficient of the error
ρ	= density
$\sigma_k, \sigma_\epsilon$	= k–ϵ model constants
τ	= stress tensor
∇	= gradient
$\nabla\cdot$	= divergence

Subscripts

av	= average
h	= finite element solution
T	= turbulent
∂, B	= boundary
0	= initial value

Introduction

ADAPTIVE finite element methods provide a powerful approach for tackling complex computational fluid dynamics problems. They can provide accurate solutions at a reasonable cost by automatically clustering elements around flow features of interest such as shear and boundary layers and reattachment points. Such an adaptive process is cost effective in the sense that the best numerical solution is obtained at the least computational cost. Moreover, such approaches provide flexibility in modeling and algorithm development. The ability of the methodology to produce uniformly accurate solutions makes it possible to obtain numerically exact solutions to the equations of motion, so that mathematical models of the physical phenomenon of interest can be evaluated with confidence.

Received Dec. 10, 1994; revision received Jan. 15, 1996; accepted for publication Dec. 27, 1996.

*Professor, Département de génie mécanique, P.O. Box 6079, Succursale Centre-ville. Member AIAA.

†Graduate Research Assistant, Département de génie mécanique, P.O. Box 6079, Succursale Centre-ville.

Initial breakthroughs in adaptivity were achieved in aerodynamics because of the pressing need for accurate computations of shock waves.[1] Adaptive computations on unstructured grids for aerodynamics applications are now fairly commonplace. However, for incompressible flows, the literature is not as abundant. Proof of concept computations for laminar incompressible flow were reported in Refs. 2 and 3. An early paper discussing adaptivity and the k–ϵ model is that of Moukalled and Acharya,[4] where structured grids are adapted by both moving nodes and imbedding a finer grid in the coarser one. The methodology proposed here uses unstructured grids to provide for very high localized grid resolution at a reasonable cost. The remeshing procedure makes it possible to achieve any preset level of accuracy. Thus, the method can be viewed as a technique for generating numerically exact solutions to the differential equations modeling turbulent flow. In Refs. 5–8 the methodology proposed was quantitatively validated by solving laminar flows with known analytical solutions and by computing cases for which experimental measurements were available. The methodology was further extended to convective heat transfer flows with variable fluid properties[9] and to zero-equation models of turbulence for free shear flows.[10]

This paper presents an extension of the methodology to turbulent free shear flows. The methodology is based on adaptive remeshing coupled to a finite element solver for steady-state incompressible turbulent flows for which turbulence is represented by the k–ϵ model. The paper is organized as follows. We describe the modeling of the problem. The equations of motion and the finite element solver are reviewed. The turbulence model is discussed and details of the nonlinear equation solver are given. The methodology section describes two error estimators and the adaptive remeshing strategy. The proposed methodology is then validated by solving problems with known analytical solutions to clearly quantify the accuracy improvements due to adaptivity. The method is then applied to free shear flows for which experimental data are available. The paper closes with conclusions.

Modeling of the Problem

Reynolds-Averaged Navier–Stokes Equations

The flow regime of interest is modeled by the Reynolds-averaged Navier–Stokes equations

$$\rho u\cdot\nabla u = -\nabla p + \nabla\cdot[(\mu+\mu_T)(\nabla u+\nabla u^T)] + \rho f$$
$$\nabla\cdot u = 0 \tag{1}$$

where the turbulent viscosity is computed using the k–ϵ model of turbulence

$$\mu_T = \rho C_\mu (k^2/\epsilon) \tag{2}$$

The system is closed by including the transport equations for k and ϵ (Ref. 11)

$$\rho u\cdot\nabla k = \nabla\cdot\{[\mu+(\mu_T/\sigma_k)]\nabla k\} + \mu_T P(u) - \rho\epsilon \tag{3}$$

$$\rho u\cdot\nabla\epsilon = \nabla\cdot\{[\mu+(\mu_T/\sigma_\epsilon)]\nabla\epsilon\} + C_1(\epsilon/k)\mu_T P(u) - C_2\rho(\epsilon^2/k) \tag{4}$$

where the production of turbulence is defined as

$$P(u) = \nabla u : (\nabla u + \nabla u^T) \tag{5}$$

To ensure an efficient iterative solution of the equations, the k and ϵ transport equations were rewritten in the following way. The turbulent viscosity multiplying the production in the ϵ equation is expressed in terms of k and ϵ, and the turbulence dissipation ϵ is replaced in the k equation by using the following identity:

$$\epsilon = \rho C_\mu (k^2/\mu_T) \tag{6}$$

We then obtain the following equations, which are formally equivalent to Eqs. (3) and (4):

$$\rho u \cdot \nabla k = \nabla \cdot \{[\mu + (\mu_T/\sigma_k)]\nabla k\} + \mu_T P(u) - \rho^2 C_\mu (k^2/\mu_T) \tag{7}$$

$$\rho u \cdot \nabla \epsilon = \nabla \cdot \{[\mu + (\mu_T/\sigma_\epsilon)]\nabla \epsilon\} + \rho C_1 C_\mu k P(u) - C_2 \rho (\epsilon^2/k) \tag{8}$$

The constants C_μ, C_1, C_2, σ_k, and σ_ϵ take on the standard values proposed in Ref. 11.

This set of differential equations is solved in a partly segregated manner using the following algorithm: 1) given u_0, k_0, ϵ_0; 2) compute μ_T from k and ϵ; 3) for μ_T given a) solve the momentum and continuity equations, b) solve the k equation, and c) solve the ϵ equation; and 4) update μ_T and go to step 3. This algorithm presents the following advantages.

1) Step 3a corresponds to solving the Navier–Stokes equation with variable viscosity. The proposed adaptive scheme has already proven successful for such problems.[9]

2) Steps 3b and 3c are solved in turn using the most recent values of u and k. They contain only quadratic nonlinearities in k^2 and ϵ^2, respectively.

Finite Element Solver

The finite element equations are obtained by multiplying the differential equations by suitable test functions and performing integration by parts of diffusion terms. This leads to the following Galerkin variational equations.

Momentum and continuity:

$$\begin{gathered}(\rho u \cdot \nabla u, v) + a(u, v) - (p, \nabla \cdot v) = (f, v) + \langle \hat{t}, v \rangle \\ (q, \nabla \cdot u) = 0\end{gathered} \tag{9}$$

with

$$(h, g) = \int_\Omega hg \, d\Omega \qquad a(u, v) = \int_\Omega 2(\mu + \mu_T)\dot{\gamma}(u) : \dot{\gamma}(v) \, d\Omega$$

$$\dot{\gamma}(u) = \frac{\nabla u + \nabla u^T}{2} \tag{10}$$

$$\langle \hat{t}, v \rangle = \int_{\partial K \setminus \Gamma_t} [2(\mu + \mu_T)\dot{\gamma}(u) \cdot n - pn] \cdot v \, ds + \int_{\partial K \cap \Gamma_t} \hat{t} \cdot v \, ds$$

where v is the test function. The double contraction is defined as follows:

$$\dot{\gamma}(u) : \dot{\gamma}(v) = \sum_i \sum_j \dot{\gamma}_{ij}(u)\dot{\gamma}_{ij}(v)$$

$$= \sum_i \sum_j \left[\frac{\partial u_i}{\partial x_j} + \frac{\partial u_j}{\partial x_i}\right]\left[\frac{\partial v_i}{\partial x_j} + \frac{\partial v_j}{\partial x_i}\right]$$

Turbulence kinetic energy (step 3b):

$$\int_\Omega \left[\rho u \cdot \nabla k w + \left(\mu + \frac{\mu_T}{\sigma_k}\right)\nabla k \cdot \nabla w + \rho^2 C_\mu \frac{k^2}{\mu_T} w\right] d\Omega = \int_\Omega \mu_T P(u) w \, d\Omega \tag{11}$$

Turbulence dissipation (step 3c):

$$\int_\Omega \left[\rho u \cdot \nabla \epsilon s + \left(\mu + \frac{\mu_T}{\sigma_\epsilon}\right)\nabla \epsilon \cdot \nabla s + \rho C_2 \frac{\epsilon^2}{k} s\right] d\Omega = \int_\Omega \rho C_1 C_\mu k P(u) s \, d\Omega \tag{12}$$

These equations are solved in primitive variables using an augmented Lagrangian algorithm to treat the incompressibility.[12] The equations are discretized with the Crouzeix–Raviart triangular element, which uses an enriched quadratic velocity approximation and a linear discontinuous pressure. A standard quadratic interpolant is used for k and ϵ.

Adaptive Methodology

Generalities

Most adaptive methods assess the quality of an initial solution obtained on a coarse mesh by using some form of error estimation and modifying the structure of the numerical approximation in a systematic fashion to improve the overall quality of the solution. There are several ways of achieving adaptivity: P methods increase the degree of polynomial approximations for improved accuracy,[13] R methods relocate grid points in regions of rapid change of the solution,[14] and H methods proceed by either mesh enrichment or remeshing.[1,5]

A variant of an H method, called adaptive remeshing, has been retained because it provides the greatest control of element size and grading to accurately resolve flow features such as shear and thermal layers, stagnation points, jets, and wakes. In this approach the problem is first solved on a coarse grid to roughly capture the physics of the flow. The resulting solution is then analyzed to determine where more grid points are needed, and an improved mesh is generated. The problem is solved again on the new mesh using the solution obtained on the coarser mesh as an initial guess. This process is repeated until the required level of accuracy is achieved.

Remeshing also offers an elegant and simple approach to overcome some of the obstacles specific to incompressible viscous flows. For instance, the best proven finite element approximations can be selected based on their convergence and accuracy properties.[12,15] This circumvents the problem associated with P methods of satisfying the so-called Babuska compatibility condition between the velocity and pressure approximations.[12,15] It also eliminates the hanging node problem encountered in some H-refinement methods.[3]

Error Estimation

This section describes two error estimation techniques for assessing the accuracy of the solutions obtained by the finite element solver.

Projection Error Estimator

This error estimator was first introduced by Zienkiewicz and Zhu[16] and involves postprocessing of the strain rate tensor $\dot{\gamma} = (\nabla u + \nabla u^T)/2$. The method is based on the observation that whereas the true derivatives are continuous throughout the flow domain, the finite element derivatives $\dot{\gamma}_h$ are discontinuous across element faces. The theory of the finite element method also states that $\dot{\gamma}_h$ converges to its true value as the mesh is refined. Hence, a measure of the quality of the velocity prediction can be obtained by computing the norm of $(\dot{\gamma}_h - \dot{\gamma}_{ex})$, where $\dot{\gamma}_h$ and $\dot{\gamma}_{ex}$ are the finite element and exact strain rates, respectively.

Unfortunately, the exact solution is not available in practice. However, it has been shown that the exact derivatives can be replaced by a continuous least-squares approximation (see Refs. 16 and 17 for details). Thus, the velocity error e^u can be estimated by

$$\|e^u\|_{E,\Omega} = \left\{\int_\Omega (\tilde{\gamma} - \dot{\gamma}_h) : (\tilde{\gamma} - \dot{\gamma}_h) \, d\Omega\right\}^{\frac{1}{2}} \tag{13}$$

Here $\tilde{\gamma}$ is the continuous least-squares projection of $\dot{\gamma}_h$ into the space of the velocity interpolation functions. This approach can be extended to include the pressure error

$$\|e^p\|_{0,\Omega} = \left\{ \int_\Omega (\tilde{p} - p_h)^2 \, d\Omega \right\}^{\frac{1}{2}} \tag{14}$$

where $\tilde{p}$ is the continuous piecewise linear least-squares fit to p_h, the finite element discontinuous pressure.

The error contributions from the turbulence equations are incorporated in a similar manner. The errors in k and ϵ are then computed by evaluating

$$\|e^k\|_{E,\Omega} = \left\{ \int_\Omega (\tilde{q}_{k_h} - q_{k_h}) \cdot (\tilde{q}_{k_h} - q_{k_h}) \, d\Omega \right\}^{\frac{1}{2}} \tag{15}$$

$$\|e^\epsilon\|_{E,\Omega} = \left\{ \int_\Omega (\tilde{q}_{\epsilon_h} - q_{\epsilon_h}) \cdot (\tilde{q}_{\epsilon_h} - q_{\epsilon_h}) \, d\Omega \right\}^{\frac{1}{2}} \tag{16}$$

where $q_k = \nabla k$ and $q_\epsilon = \nabla \epsilon$. An error estimator is also constructed for the eddy viscosity since smooth fields of k and ϵ can result in an eddy viscosity presenting rapid variations or fronts. Such fronts in μ_T determine the turbulent diffusion of momentum and k. Thus, the accuracy of μ_T is critical to that of u, k, and ϵ. The error estimator for μ_T is defined as

$$\|e^{\mu_T}\|_{E,\Omega} = \left\{ \int_\Omega (\tilde{q}_{\mu_{T_h}} - q_{\mu_{T_h}}) \cdot (\tilde{q}_{\mu_{T_h}} - q_{\mu_{T_h}}) \, d\Omega \right\}^{\frac{1}{2}} \tag{17}$$

where $q_{\mu_T} = \nabla \mu_T$.

The total error is then computed as

$$\|(e^u, e^p, e^k, e^\epsilon, e^{\mu_T})\|_\Omega = \{ \|e^u\|^2_{E,\Omega} + \|e^p\|^2_{0,\Omega} + \|e^k\|^2_{E,\Omega} + \|e^\epsilon\|^2_{E,\Omega} + \|e^{\mu_T}\|^2_{E,\Omega} \}^{\frac{1}{2}} \tag{18}$$

Note that k, ϵ, and μ_T generally take values that are several orders of magnitude smaller than the velocity. Hence, their error estimates will be much smaller than those of u. However, both k and ϵ directly affect u through their ratio $\mu_T = \rho C_\mu k^2/\epsilon$. Thus, an accurate solution for both k and ϵ is required to obtain a meaningful velocity field. To ensure that turbulence errors are of the same order as the velocity errors, the velocity and turbulence fields are scaled so that all error maxima are of the same order of magnitude.

Local Variational Problem for the Error

This approach eliminates the global least-squares problem of the projection estimator and has the added advantage of being more general than the preceding one. The exact solution (u, p, k, ϵ) satisfies the following variational equations on each element:

$$(\rho \bar{u} \cdot \nabla u, v)_K + a(u, v)_K - (p, \nabla \cdot v)_K = (\rho f, v)_K + \langle 2(\mu + \mu_T)\dot{\gamma}(u) \cdot n - p \, n, v \rangle_{\partial K \setminus \Gamma_{\hat{t}}} + \langle \hat{t}, v \rangle_{\partial K \cap \Gamma_{\hat{t}}} \quad \forall v \in \mathcal{P}^p(K)$$
$$(q, \nabla \cdot u)_K = 0, \qquad \forall q \in \mathcal{L}^1(K) \tag{19}$$

$$(\rho \bar{u} \cdot \nabla k, w)_K + b(k, w)_K - [\mu_T P(\bar{u}), w]_K + [\rho^2 C_\mu (k^2/\mu_T), w]_K = \langle [\mu + (\mu_T/\sigma_k)] \nabla k \cdot n, w \rangle_{\partial K \setminus \Gamma_{\hat{q}_k}} + \langle \hat{q}_k, w \rangle_{\partial K \cap \Gamma_{\hat{q}_k}}, \qquad \forall w \in \mathcal{T}^k(K) \tag{20}$$

$$(\rho \bar{u} \cdot \nabla \epsilon, s)_K + c(\epsilon, s)_K - [\rho C_1 C_\mu k P(\bar{u}), s]_K + [\rho C_2 (\epsilon^2/k), s]_K = \langle [\mu + (\mu_T/\sigma_\epsilon)] \nabla \epsilon \cdot n, s \rangle_{\partial K \setminus \Gamma_{\hat{q}_\epsilon}} + \langle \hat{q}_\epsilon, s \rangle_{\partial K \cap \Gamma_{\hat{q}_\epsilon}}, \qquad \forall s \in \mathcal{L}^1(K) \tag{21}$$

where

$$a(u, v)_K = \int_{\Omega_K} 2(\mu + \mu_T)\dot{\gamma}(u) : \dot{\gamma}(v) \, d\Omega \tag{22}$$

$$b(k, w)_K = \int_{\Omega_K} \left[\mu + \frac{\mu_T}{\sigma_k} \right] \nabla k \cdot \nabla w \, d\Omega \tag{23}$$

$$c(\epsilon, s)_K = \int_{\Omega_K} \left[\mu + \frac{\mu_T}{\sigma_\epsilon} \right] \nabla \epsilon \cdot \nabla s \, d\Omega \tag{24}$$

Here $\partial K \setminus \Gamma_{\hat{t}}$ denotes the element faces not on the region of the domain boundary where tractions are imposed and $\partial K \cap \Gamma_{\hat{t}}$ denotes the element faces located on the region of the boundary where tractions are imposed. $\mathcal{P}^p(K)$ denotes the space of velocity functions on element K, $\mathcal{T}^k(K)$ denotes the space of turbulence kinetic energy (TKE) functions on element K, and $\mathcal{L}^1(K)$ denotes the space of ϵ functions on element K.

By substituting the following relationships between the true solution, its finite element approximation and the errors,

$$u = u_h + e^u_h, \qquad p = p_h + e^p_h$$
$$k = k_h + e^k_h, \qquad \epsilon = \epsilon_h + e^\epsilon_h \tag{25}$$

we obtain the following variational equations for the components of the error over an element.

Momentum error:

$$a(e^u_h, v_h)_K - (e^p_h, \nabla \cdot v_h)_K = -a(u_h, v_h)_K + (\rho f - \rho u_h \cdot \nabla u_h, v_h)_K + (p_h, \nabla \cdot v_h)_K + \langle 2(\mu + \mu_T)\dot{\gamma}(u_h) \cdot n - p_h \, n, v_h \rangle_{\partial K \setminus \Gamma_{\hat{t}}} + \langle \hat{t}, v_h \rangle_{\partial K \cap \Gamma_{\hat{t}}}, \qquad \forall v_h \in \mathcal{P}^p(K) \tag{26}$$

Continuity error:

$$(q_h, \nabla \cdot e^u_h)_K = -(q_h, \nabla \cdot u_h)_K, \qquad \forall q_h \in \mathcal{L}^1(K) \tag{27}$$

TKE error:

$$b(e^k_h, w_h)_K + [2\rho^2 C_\mu (k_h/\mu_T) e^k_h, w_h]_K = -b(k_h, w_h)_K + (-\rho u_h \cdot \nabla k_h + \mu_T P(u_h) - \rho \epsilon_h, w_h)_K + \langle [\mu + (\mu_T/\sigma_k)] \nabla k_h \cdot n, w_h \rangle_{\partial K \setminus \Gamma_{\hat{q}_k}} + \langle \hat{q}_k, w_h \rangle_{\partial K \cap \Gamma_{\hat{q}_k}}, \qquad \forall w_h \in \mathcal{T}^k(K) \tag{28}$$

TKE dissipation error:

$$c(e^\epsilon_h, s_h)_K + [2\rho C_2 (\epsilon_h/k_h) e^\epsilon_h, s_h]_K = -c(\epsilon_h, s_h)_K + [-\rho u_h \cdot \nabla \epsilon_h + \rho C_1 C_\mu k_h P(u_h) - \rho C_2 (\epsilon_h^2/k_h), s_h]_K + \langle [\mu + (\mu_T/\sigma_\epsilon)] \nabla \epsilon_h \cdot n, s_h \rangle_{\partial K \setminus \Gamma_{\hat{q}_\epsilon}} + \langle \hat{q}_\epsilon, s_h \rangle_{\partial K \cap \Gamma_{\hat{q}_\epsilon}}, \qquad \forall s_h \in \mathcal{L}^1(K) \tag{29}$$

Convective terms of the form $e^u_h \cdot \nabla e^u_h$, $e^u_h \cdot \nabla u_h$, and $u_h \cdot \nabla e^u_h$ have been neglected, following Ref. 17. The remaining nonlinear terms have been linearized. The flux terms on the element sides are approximated by the average value of the raw finite element fluxes. The terms in parentheses on the right-hand sides are the element residuals, a measure of the accuracy of the finite element solution inside the element. This variational problem is discretized locally on each element. Errors in u, v, k, and ϵ are discretized using quartic bubble functions defined on the element sides. Pressure errors are approximated by a nonconforming quadratic bubble function. This results in small 13×13 systems of linear equations on each element. The turbulent viscosity error is evaluated from the TKE and dissipation errors by using the following expression:

$$e^{\mu_T}_h = \mu_{T_h} [2(e^k_h/k_h) - (e^\epsilon_h/\epsilon_h)] \tag{30}$$

Finally, the norms of the errors on each element are computed with the expressions defined in the preceding section.

Adaptive Remeshing

There remains one key issue to discuss: How does one exploit the knowledge of the error distribution to design a better mesh? The adaptive remeshing strategy is straightforward, follows that proposed by Peraire et al.,[1] and proceeds as follows.

1) Generate an initial mesh.
2) Compute the finite element solution.

3) Compute error estimate.
4) If (global error < tolerance), then
stop;
else
compute grid density from error estimate
generate an improved mesh according to grid density
interpolate current solution on new mesh;
goto step 2;
end if.

We now provide details on some of the steps of this algorithm. Once the finite element solution has been obtained, the error on each element is computed using either one of the previously described estimators. The global norms of the solution and the error are computed as follows:

$$\|e_{\text{tot}}\|^2 = \sum \|e_k\|^2 \tag{31}$$

There remains to compute the element size for the improved mesh so that elements are smaller in regions of large error and bigger in regions where the solution is already accurate. This is achieved by requiring that the improved mesh be optimal (i.e., that all elements have the same average error e_{av}). Now, given a target reduction coefficient of the error ξ, the total and average error can be related as follows:

$$\|e_{\text{av}}\| = \xi \frac{\|e_{\text{tot}}\|}{\sqrt{n}} \tag{32}$$

Finally, an expression for the element size δ can be derived from the asymptotic rate of convergence of the finite element approximation

$$\delta = \left[\frac{\xi \|e_{\text{tot}}\|}{\|e\| \sqrt{n}} \right]^{1/k} h \tag{33}$$

(see Refs. 5 and 6 for details).

This distribution of the element size is then used as the grid function in an advancing front mesh generator[1] to generate an improved mesh.

Validation: Two-Dimensional Shear Layer

The error estimators are first compared on a simple flow problem for which an analytical solution is known. This provides controlled conditions for validating the methodology and assessing its computational performance.

Convergence was achieved when the relative norm of the correction between two successive global iterates was less than 10^{-6}. In all cases subiterations on u, k, and ϵ were performed until the relative error and the L_2 norms of residuals were of the order 10^{-6}. In all cases the adaptive procedure and finite element code were run in a blackbox fashion with no intervention on the part of the user. The adaptive procedure was set to reduce the global error by a factor of 3 at each cycle of adaptation.

This is a variant of the shear layer[18] between two coflowing streams of velocity, U_1 and U_2, for which the turbulent viscosity is linear in x. The solution is taken to be

$$\begin{aligned} u &= \left[\frac{u_1 + u_2}{2} \right] + \left[\frac{u_1 - u_2}{2} \right] \operatorname{erf}\left(\frac{\sigma y}{x} \right) \\ v &= -\left[\frac{u_1 - u_2}{2} \right] \frac{1}{\sigma \sqrt{\pi}} \exp\left[-\left(\frac{\sigma y}{x} \right)^2 \right] \\ p &= 0 \\ k &= k_0 \{ c + \exp[-(\sigma y / x)^2] \} \\ \epsilon &= (\epsilon_0 / x) \{ c + \exp[-(\sigma y / x)^2] \}^2 \end{aligned} \tag{34}$$

The velocity ratio $r = u_2/u_1$ was set to zero. These expressions are substituted in Eqs. (1–4) to determine the appropriate source terms. This problem presents all of the features of the experimental observations of Refs. 19 and 20. The computational domain is the rectangle $[100, 300] \times [-50, 50]$.

Figure 1 illustrates the trajectory generated by the estimators. Both error estimators drive the adaptation process to reduce the error and its estimate at each cycle. Hence, the solution accuracy improves steadily at each adaptation cycle. Both estimators behave similarly. Figure 2 shows a typical histogram of the elemental error. It represents a count of the elements having the same level of error. In an ideal situation all elements would have the same error. In practice, we obtain an approximately Gaussian distribution. As can be seen from Fig. 2, the error is reduced throughout the domain. Furthermore, the proportion of the elements clustered near the mean increases from one cycle to the other indicating that the meshes tend toward optimality.

Figure 3 illustrates the mesh generated by the procedure. In both cases the adaptation strategy proceeds by a complete reallocation of grid points, refining the mesh around the fronts of k and near the center of the shear layer in the midsection of the domain. Contour lines of the eddy viscosity are presented in Fig. 4. Figure 4a represents the solution obtained on the initial coarse mesh, whereas Fig. 4b presents the solution on the final mesh. The quality of the prediction of the turbulent viscosity improves drastically between the initial and final meshes. Contours are equally spaced between values of 0.13 and 0.42.

Figure 5 presents a qualitative comparison of contour lines of the combined error for both estimators. Contours of the true errors are

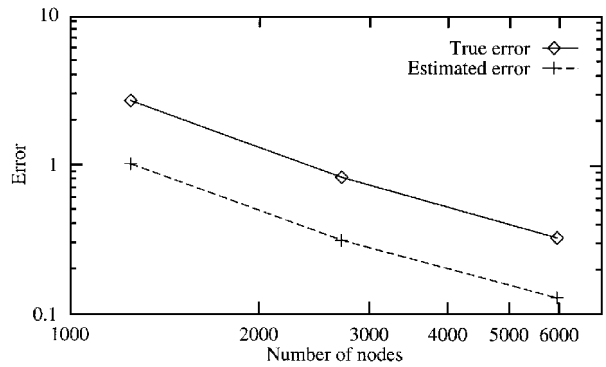

Projection estimators

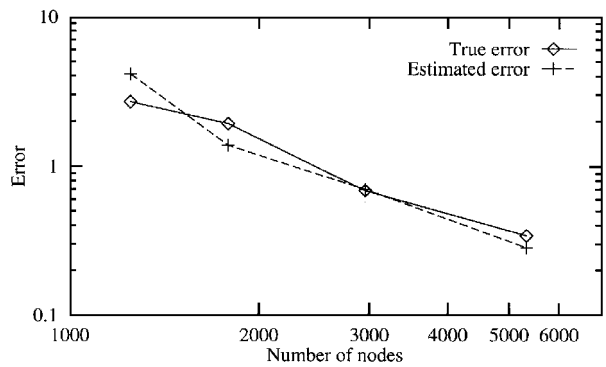

Local problem estimator

Fig. 1 Trajectory generated by the estimators.

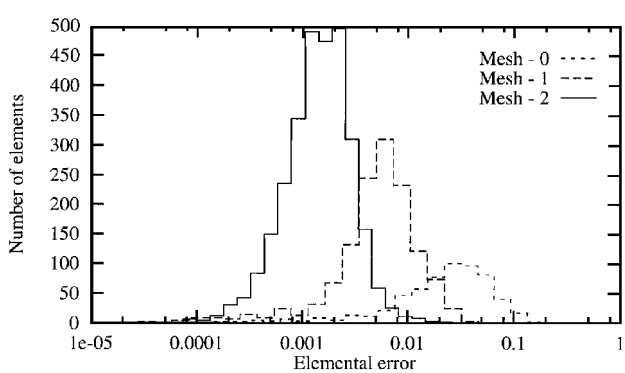

Fig. 2 Histogram of the element error: projection estimator.

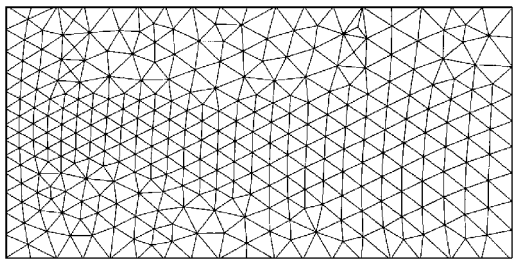

Mesh 0

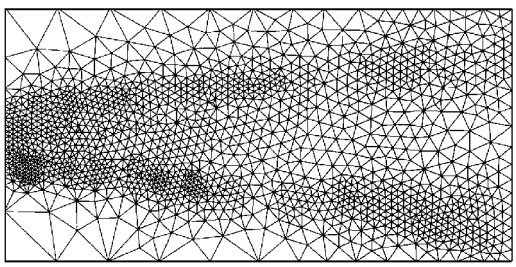

Mesh 2

Fig. 3 Meshes generated by the projection.

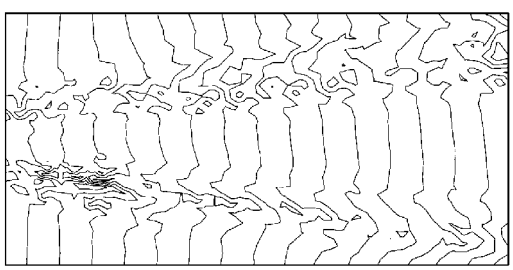

a) Mesh 0

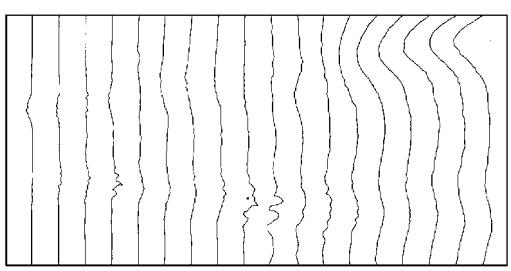

b) Mesh 2

Fig. 4 Eddy viscosity obtained on the initial and final meshes.

shown in Figs. 5a and 5c, whereas those of the estimators are in Figs. 5b and 5d. One can see that the error estimators reproduce the key features of the true error: peaks and valley regions of high and low errors are detected in the same locations.

Application to a Planar Shear Layer with $U_2/U_1 = 0.3$

This problem was the subject of an experimental investigation by Spencer and Jones[21] and has many features in common with the flow past the trailing edge of an airfoil. The far field of this flow has been simulated by Duncan et al.[22] using the k–ϵ model and several of its multiple time-scale variants. Figure 6 presents the geometry and boundary conditions used for the present study which includes the trailing edge region of the splitter plate and the near field of the wake. The Reynolds number is $U_1/\nu = 2 \cdot 10^4$/cm. Coordinates are dimensionless, and the reference length is 1 cm. The domain is the rectangle $[-10, 120] \times [-30, 30]$ and includes the splitter plate ($x = -10$ to 0).

The local problem estimator did not provide solution improvement on this practical flow problem. This may be due to the use of streamline upwinding in the solver, which is not accounted for by this estimator. Therefore, only the projection error estimator was used for this application.

Figure 7 presents the adaptively generated meshes for the complete computational domain. Notice the diagonal bands of element concentration, which coincide with the fronts of k and μ_T. Grid points have also been tightly clustered around the trailing edge of the plate where all variables undergo rapid variations.

Figure 8 presents a comparison of predicted and measured streamwise velocity profiles at two control stations located at 25 and 50 cm from the trailing edge. All curves are plotted in similarity variables. It is known that the use of such variables tends to mask differences. The data from Spencer and Jones[21] were given in this form with insufficient information to extract true values and coordinates. As can be seen, predictions are good and the improvements due to adaptivity

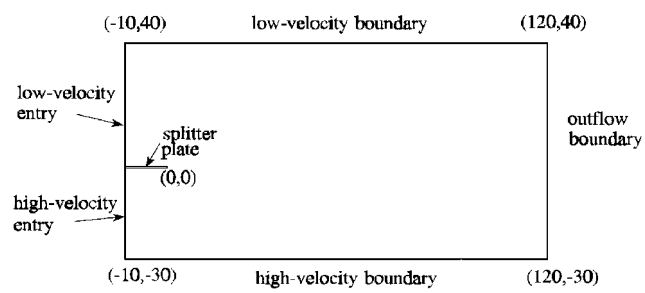

Fig. 6 Domain and boundary conditions for the shear layer of Spencer and Jones.[21]

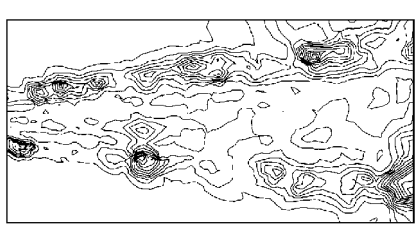

a) True error

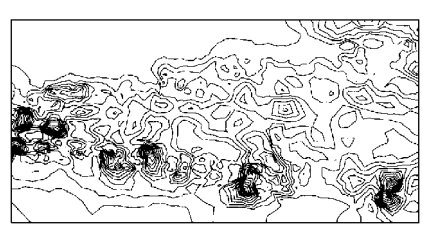

c) True error

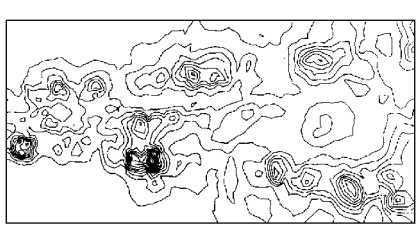

b) Projection estimator

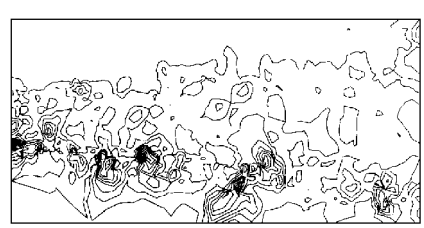

d) Local problem estimator

Fig. 5 Contour lines of the errors.

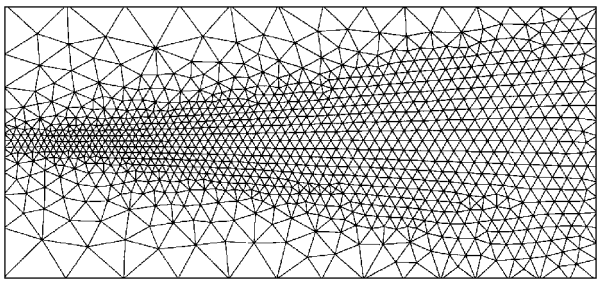

Initial mesh

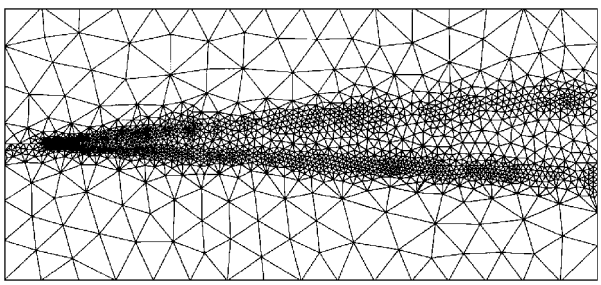

Final mesh

Fig. 7 Meshes generated by the adaptive procedure.

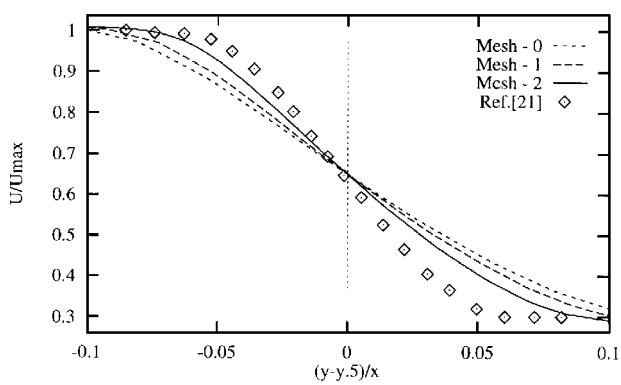

$x = 25$ cm

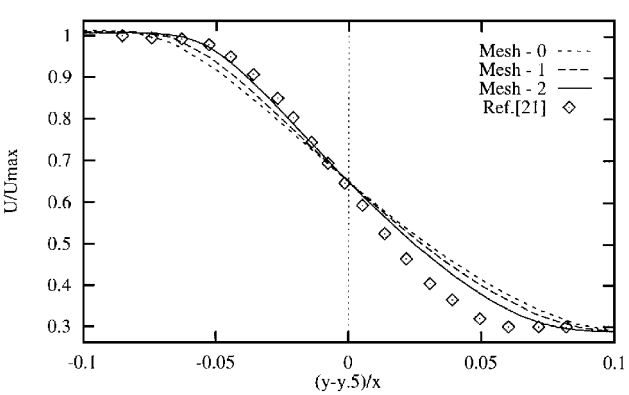

$x = 50$ cm

Fig. 8 Velocity profiles.

are most pronounced at the first station. The improvements are even more evident in the profiles of the turbulent kinetic energy shown in Fig. 9. At $x = 25$ cm, a reduction of 20% in the predicted peak value due to adaptive mesh refinement results in significantly better agreement with the measurements. At $x = 50$ cm, the change in peak value is roughly 5%, but the width of the shear layer has decreased significantly to be in closer agreement with the measurements.

Finally, Fig. 10 presents a comparison of predicted and measured Reynolds stress profiles. Because they are derived quantities, Reynolds stresses are predicted with less accuracy than primary

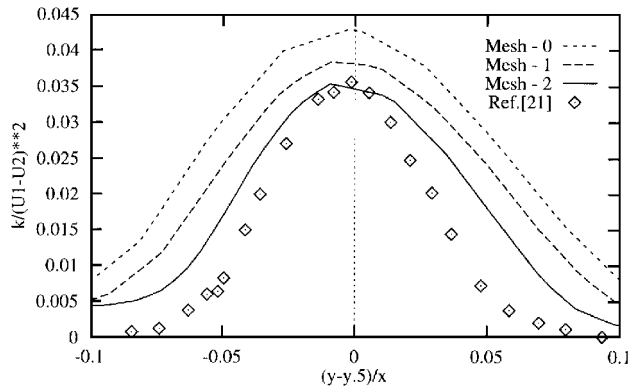

$x = 25$ cm

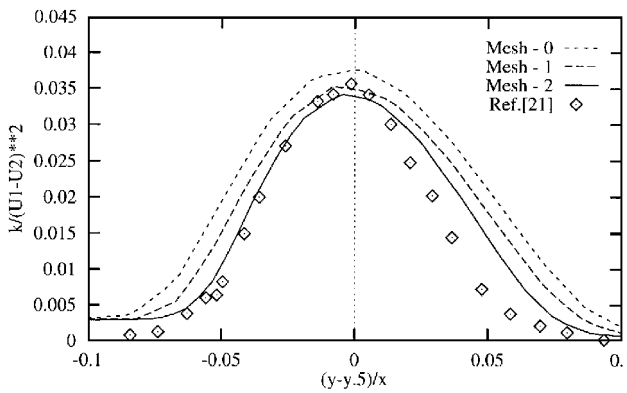

$x = 50$ cm

Fig. 9 Turbulence kinetic energy profiles.

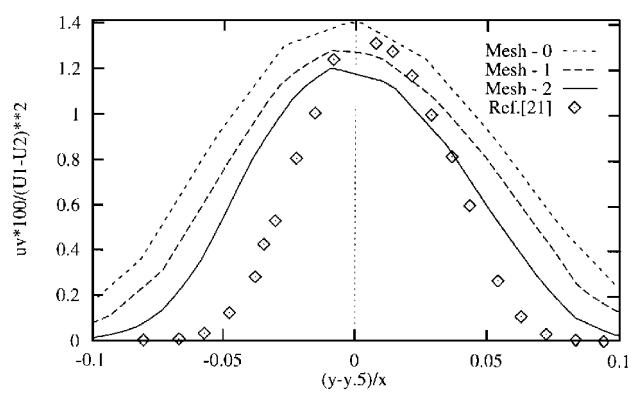

$x = 25$ cm

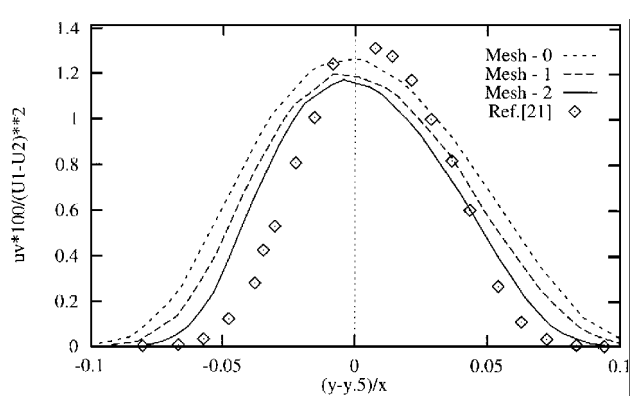

$x = 50$ cm

Fig. 10 Reynolds stress distribution.

variables, such as velocity, and should benefit more from adaptive refinement. Figure 10 confirms this observation. Here again improvements due to adaptivity are most evident in the near-field region where the shear layer is thinnest and solution variations are largest.

Conclusions

An adaptive remeshing finite element procedure has been presented for solving turbulent free shear flows using the k–ϵ model of turbulence.

The finite element solution algorithm has proven very robust and reliable. Generally speaking, once a solution has been obtained on the initial coarse mesh (requiring approximately 25 global iterations), about 3 or 4 global iterations are required on the subsequent meshes and at most 2 inner iterations are performed for the momentum, k, and ϵ equations. Thus, the use of adaptivity results in significant computational saving.

The two proposed error estimators have proven reliable and convergent on nontrivial problems having analytical solution. However, for now, only the projection method has proven useful on practical cases. For the shear layer, the agreement with measurements improves with each cycle of adaptation. Improvement is most important in the near field where the variables exhibit the most rapid variations.

The adaptive procedure appears robust. It can be used in a black-box fashion with little or no intervention on the part of the user and leads to improved accuracy and overall computational efficiency.

Acknowledgments

The authors would like to acknowledge the financial support of the National Sciences and Engineering Research Council of Canada and by Direction des Études et Recherches d'Électricité de France with J.-P. Chabard as Technical Monitor.

References

[1]Peraire, J., Vahdati, M., Morgan, K., and Zienkiewicz, O. C., "Adaptive Remeshing for Compressible Flows," *Journal of Computational Physics*, Vol. 72, No. 2, 1987, pp. 26–37.

[2]Wu, J., Zhu, J. Z., Szmelter, J., and Zienkiewicz, O. C., "Error Estimation and Adaptivity in Navier–Stokes Incompressible Flows," *Computational Mechanics*, Vol. 6, No. 3, 1990, pp. 259–270.

[3]Wang, K. C., and Carey, G. F., "Adaptive Grids for Coupled Viscous Flow and Transport," *Computer Methods in Applied Mechanics and Engineering*, Vol. 82, No. 3, 1990, pp. 365–383.

[4]Moukalled, F., and Acharya, S., "Application of an Adaptive Grid Procedure for the Calculation of Turbulent Separated Flows," *Computers and Fluids*, Vol. 21, No. 3, 1992, pp. 455–473.

[5]Hétu, J.-F., and Pelletier, D., "Adaptive Remeshing for Viscous Incompressible Flows," *AIAA Journal*, Vol. 30, No. 8, 1992, pp. 1986–1992.

[6]Hétu, J.-F., and Pelletier, D., "A Fast Adaptive Finite Element Scheme for Viscous Incompressible Flows," *AIAA Journal*, Vol. 30, No. 11, 1992, pp. 68–75.

[7]Pelletier, D., and Hétu, J.-F., "An Adaptive Finite Element Methodology for Incompressible Viscous Flows," *Advances in Finite Element Analysis in Fluid Mechanics, ASME Winter Annual Meeting (Anaheim, CA)*, edited by M. N. Dhaubhadel, M. S. Engelman, and J. N. Reddy, FED-Vol. 137, American Society of Mechanical Engineers, Nov. 1992.

[8]Pelletier, D., Hétu, J.-F., and Ilinca, F., "An Adaptive Finite Element Method for Thermal Flow Problems," *AIAA Journal*, Vol. 32, No. 4, 1994, pp. 741–747.

[9]Pelletier, D., Ilinca, F., and Hétu, J.-F., "An Adaptive Finite Element Method for Convective Heat Transfer with Variable Fluid Properties," *Journal of Thermophysics and Heat Transfer*, Vol. 8, No. 4, 1994, pp. 687–694.

[10]Pelletier, D., Ilinca, F., and Hétu, J.-F., "An Adaptive Finite Element Method for Turbulent Free Shear Flow Past a Propeller," *AIAA Journal*, Vol. 32, No. 11, 1994, pp. 2186–2193.

[11]Launder, B. E., and Spalding, J., "The Numerical Computation of Turbulent Flows," *Computer Methods in Applied Mechanics and Engineering*, Vol. 3, No. 2, 1974, pp. 269–289.

[12]Pelletier, D., and Fortin, A., "Are FEM Solutions of Incompressible Flows Really Incompressible? (or How Simple Flows Can Cause Headaches)," *International Journal for Numerical Methods in Fluids*, Vol. 9, No. 1, 1989, pp. 99–112.

[13]Zienkiewicz, O. C., Gago, J. P., and Kelley, D. W., "The Hierarchical Concepts in Finite Element Analysis," *Computers and Structures*, Vol. 16, 1983, pp. 53–65.

[14]Lohner, R., Morgan, K., and Zienkiewicz, O. C., "Adaptive Grid Refinement for the Euler and Compressible Navier–Stokes Equations," *Accuracy Estimates and Adaptive Refinement in Finite Element Computations,* Wiley, New York, 1986.

[15]Fortin, M., and Fortin, A., "Experiments with Several Elements for Incompressible Flows," *International Journal for Numerical Methods in Fluids*, Vol. 5, No. 9, 1985, pp. 911–928.

[16]Zienkiewicz, O. C., and Zhu, R. J. Z., "A Simple Error Estimator and Adaptive Procedure for Practical Engineering Analysis," *International Journal for Numerical Methods in Engineering*, Vol. 24, No. 2, 1987, pp. 337–357.

[17]Hétu, J. F., "Méthodes d'éléments finis adaptatives pour les écoulements visqueux incompressibles," Ph.D. Thesis, École Polytechnique de Montréal, Montréal, PQ, Canada, Dec. 1991.

[18]Schlichting, H., *Boundary Layer Theory*, 7th ed., McGraw–Hill, New York, 1979, pp. 737–739.

[19]Wygnanwski, I., and Fiedler, H. E., "The Two-Dimensional Mixing Region," *Journal of Fluid Mechanics*, Vol. 41, Pt. 2, 1970, pp. 327–361.

[20]Patel, R., "An Experimental Study of a Plane Mixing Layer," *AIAA Journal*, Vol. 11, No. 1, 1973, pp. 67–71.

[21]Spencer, B. W., and Jones, B. G., "Statistical Investigation of Pressure and Velocity Fields in the Turbulent Two-Stream Mixing Layer," AIAA Paper 71-0613, June 1971.

[22]Duncan, B. S., Liou, W. W., and Shih, T. H., "A Multiple-Scale Turbulence Model for Incompressible Flow," AIAA Paper 93-0086, Jan. 1993.

F. W. Chambers
Associate Editor